Neutral-particle production in $\pi^- p$ interactions at 147 GeV/c and comparison to charged-particle production

D. Brick, D. Fong,* M. Heller,† A. M. Shapiro, and M. Widgoff
Brown University, Providence, Rhode Island 02912

F. Bruyant
CERN, Geneva 23, Switzerland

D. Bogert and M. Johnson
Fermilab, Batavia, Illinois 60510

R. Burnstein, C. Fu,‡ D. Petersen,§ M. Robertson,‖ and H. Rubin
Illinois Institute of Technology, Chicago, Illinois 60616

R. Sard, A. Snyder,¶ and J. Tortora**
University of Illinois, Urbana, Illinois 61801

E. D. Alyea, Jr.
Indiana University, Bloomington, Indiana 47401

C.-Y. Chien, P. Lucas,†† A. Pevsner, and R. Zdanis
Johns Hopkins University, Baltimore, Maryland 21218

F. Barreiro,* O. Benary,‡‡ J. E. Brau,§§ J. Grunhaus,‡‡ E. S. Hafen, R. I. Hulsizer, U. Karshon,‖‖ V. Kistiakowsky, A. Levy,¶¶ A. Napier, I. A. Pless, J. P. Silverman,*** P. C. Trepagnier, J. Wolfson,††† and R. K. Yamamoto
Massachusetts Institute of Technology, Cambridge, Massachusetts 02139

H. Cohn
Oak Ridge National Laboratory, Oak Ridge, Tennessee 37830

P. F. Jacques, T. C. Ou, R. J. Plano, and T. L. Watts
Rutgers University, New Brunswick, New Jersey 08903

E. B. Brucker, E. L. Koller, P. Stamer, and S. Taylor
Stevens Institute of Technology, Hoboken, New Jersey 07030

W. Bugg, G. Condo, T. Handler, and E. Hart
University of Tennessee, Knoxville, Tennessee 37916

H. Kraybill, D. Ljung, T. W. Ludlam,‡‡‡ and H. D. Taft
Yale University, New Haven, Connecticut 06520

(Received 27 April 1979)

The production of K_S, Λ, $\bar{\Lambda}$, and γ in $\pi^- p$ collisions at 147 GeV/c is analyzed. Cross sections, rapidity, Feynman-x, and $p_T{}^2$ distributions are presented and compared to charged-particle production. The energy dependence of multiplicities in $\pi^- p$ and pp collisions is shown. A new scaling form for the correlation of neutral- and charged-particle multiplicities is presented for compilations of πp and pp data.

I. INTRODUCTION AND SUMMARY

We present final results on inclusive neutral-particle production in $\pi^- p$ collisions at 147 GeV/c in the 30-in. hybrid spectrometer at Fermilab,[1] and make comparisons in energy, between πp and pp collisions, between neutral- and charged-particle distributions, and among the neutral-particle results. Past studies[2] on K_S, Λ, $\bar{\Lambda}$, and γ inclusive production have established many characteristics, and here we add results at 147 GeV/c, update some comparisons, and introduce new analysis.

Inclusive cross sections in the form of average multiplicities rise with energy except for Λ production, and pp and πp multiplicities agree, again except for Λ production. The average multiplicity of Λ's per event appears to be independent of en-

ergy and less than a ratio of 2 for pp vs πp collisions as might be expected from the ratio of incoming baryons. The average K_S multiplicity agrees with the average charged-particle multiplicity as a function of energy within a constant factor. $K^{\pm}$ production does not agree.

Inclusive distributions in y, x, and $p_T{}^2$ are shown and compared to charged particle production. If a rapidity plateau is assumed for K_S production, then its height agrees with the logarithmic rise in K_S multiplicity with energy.

A new scaling function derived from Koba-Nielsen-Olesen (KNO) arguments (see later) is used to analyze the energy dependence of the semi-inclusive average multiplicity of neutral particles. The new scaling function facilitates the analysis of the data in terms of K/π ratios etc. The ratio of neutral- to charged-particle multiplicity appears to have the same form for K_S and π^0 production and to be the same for pp and πp collisions. The scaling function for the Λ multiplicity is only slightly different. The ratio of neutral- to charged-particle multiplicity is not constant as charged multiplicity increases, but does not fall for charged multiplicities above the average as expected in some models.

Section II, following, discusses experimental details, Sec. III inclusive cross sections and distributions, Sec. IV two-particle multiplicities.

II. DATA ANALYSIS

105 000 pictures were taken in this experiment, of which 97 000 were available for the study of events containing neutral decays and conversions. A first scan of the film was done for all events as defined in Ref. 3; it yielded approximately 15 000 events. A second pass was performed on events containing neutral decays and conversions to check and correct the record of the event topology and to label the neutrals according to vertex type, i.e., nonzero opening angle of decay, zero opening angle of decay in all three views, one track of pair seen to turn through 180° and to have minimum ionization throughout. The second pass was also performed on some 15% of total events which were rejected for the purposes of Ref. 3 but could not be rejected in this study of neutrals because of bias.

A completely independent scan was performed on 27 000 pictures, containing 28% of the beam flux, in order to determine the contribution of the scan losses to the cross sections, distributions, etc. The events lost from the first scan were measured carefully and their contributions to cross sections etc. increased by the factor 1/0.28. The first scan's efficiency for neutral vertices computed in the usual fashion, was 78%; the scan efficiency for the combined data in the 27 000 pictures was (98.9±0.4)%. Table I shows the sources of neutral vertices from these passes and scans.

Events found during the scan phases described above were then measured on the Rutgers PEPR.[4] Tracks from neutral decays and conversions for a all events, and charged secondary tracks from two-, four-, and six-prong events were always measured. Charged secondary tracks from events with eight or more prongs were measured only for events containing strange particles ($K_S^0, \Lambda, \bar{\Lambda}$) and only in the 27 000 sample of picutres. Data from the charged tracks are not used in the analysis in this paper.

Reconstruction of tracks in the bubble chamber and wire chambers was done by the program chain

TABLE I. Neutral-vertex counts.

	27 000 sample	70 000 sample	Total
First scan (2 passes)	733	1986	2719
Second independent scan	196		196
Total	929		2915
Total sample after cuts for decay volume, minimum length, π^- beam, etc.			2327
Neutral vertices with fits			1896
	Ambiguity resolution		
	After ionization check	After p_t cut	Final cuts
K_S^0	431	476	505
Λ	175	191	238
$\bar{\Lambda}$	17	31	32
γ	1003	1121	1121
Total resolved	1626	1819	1896
Ambiguous	270	77	0

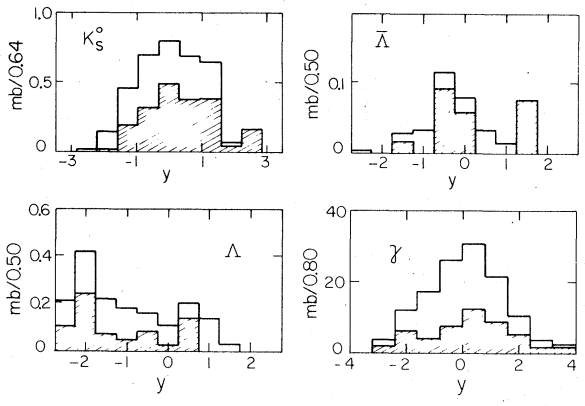

FIG. 1. Physics bias of scan and measure losses—c.m. rapidity distributions of second pass of scan and of measuring (shaded) compared to overall distribution. Events have been weighted as described in the text.

GEOMAT-PWGP-TKORG.[3] No attempt was made in this reconstruction to find parts of neutral decay tracks which entered the wire chambers—only tracks from the primary vertex were reconstructed in both bubble and wire chambers. Program SQUAW was used to identify the neutral particle using the usual three-constraint (3C) and one-constraint (1C) fits:

$$K^0_S \to \pi^+\pi^-, \tag{1a}$$

$$\Lambda \to p\pi^-, \tag{1b}$$

$$\bar{\Lambda} \to \bar{p}\pi^+, \tag{1c}$$

$$\gamma p \to e^+e^-p. \tag{1d}$$

In order to obtain satisfactory distributions of residual errors after the fit ("pull" distributions), it was necessary to increase the input error matrices on all momenta and vertex coordinates by a factor of 2 and to add constant amounts to the

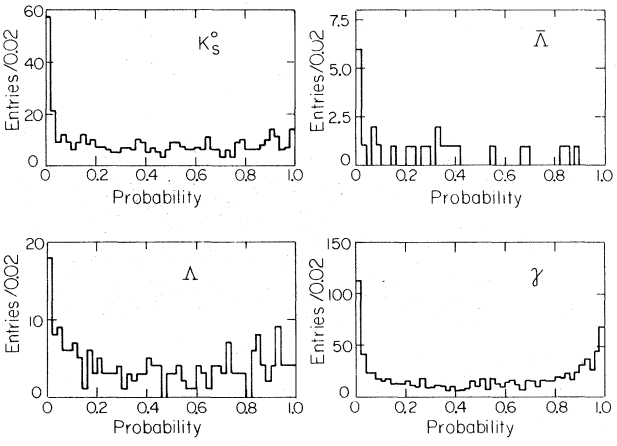

FIG. 2. χ^2 confidence level distributions for accepted 3C fits.

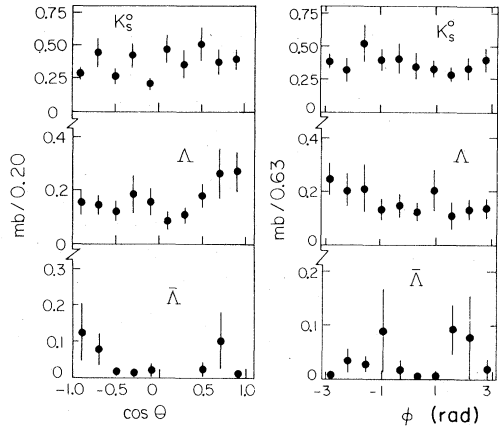

FIG. 3. Decay-angle distributions for K^0_S, Λ, $\bar{\Lambda}$. (a) $\cos\theta$ polar angle, (b) ϕ azimuthal angle. Fitted quantities have been used and distributions are weighted. Angles are calculated for the negative track in the rest frame of the neutral particle with $\hat{z}$ along the direction of the neutral and $\hat{x}$ perpendicular to the camera axis.

errors on y and z coordinates of vertices of $\Delta y = 170$ μm and $\Delta z = 850$ μm (the z direction is along the camera axis and the y direction is perpendicular to beam and z).

A decay volume cut on the decay vertex was applied at $x = 25$ cm in order to provide approximately 15 cm of visible length of decay track for reconstruction and fitting, and a minimum length cut of 2 cm was applied to neutral tracks to avoid losses of neutral vertices too close to the primary vertex. All fits were inspected at the scan table for consistency with ionization and with topological type (zero opening angle, identified electron, etc.) and for poorly measured data. Events which failed this inspection or failed to give a fit were remeasured carefully in the sample of 27 000 pictures mentioned previously and their contributions again scaled up. In

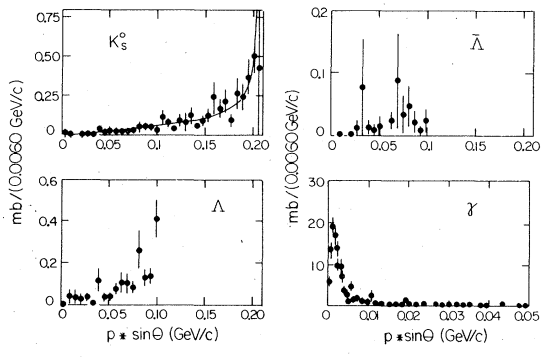

FIG. 4. Weighted distributions of momentum component of negative track from decay, transverse to line of flight of neutral. The solid line is the expected shape for K^0_S.

TABLE II. Inclusive cross sections.

	σ (mb)	Particle count
K_S^0	3.67 ± 0.38	505
Λ	1.65 ± 0.21	238
$\bar{\Lambda}$	0.38 ± 0.13	32
γ	129 ± 10.6	1121
Total		1896
	σ (mb) [a]	Pair count [a]
$K_S^0 K_S^0$	1.51 ± 0.45	28
$K_S^0 \Lambda$	0.60 ± 0.17	31
$K_S^0 \gamma$	29.7 ± 6.6	71
$\Lambda\gamma$	12.2 ± 5.7	34
$\gamma\gamma$	1000 ± 200	83

[a] See Ref. 19 for definitions of two-particle inclusive cross sections and pair counts.

this sample of 27 000 pictures, 20% of all events were remeasured because of such a measuring failure; failures occurred more often among those events with fast neutrals in the forward jet of charged particles. Figure 1 shows the c.m. rapidity distribution of the rescan and remeasured events (shaded) compared to the overall distributions; some bias towards the forward direction can be seen. About 2% of events in the 27 000 sample failed remeasurement and were not tried again.

The χ^2 probability distributions for the 3C fits which passed the decay volume cut are shown in Fig. 2; the excess of events at low probability is presumably another manifestation of the error assignment problem. Some 13% of the final accepted sample of neutrals failed to give 3C fits but gave 1C fits and were believed to point back to the primary vertex by the physicist who looked at the event on the scan table. This failure seems related to the incorrect assignment of errors on the vertices. We have included these 1C events in the cross sections and distributions since we believe their momenta are accurate enough for the studies included here.

Neutral vertices which fitted more than one decay process consistent with ionization and topology type ("ambiguous fits") were assigned by the following ordered tests:

(i) A γ fit, if present, was selected if the transverse momentum of the negative track with respect to the direction of the neutral was less than 25 MeV/c. γ fits were rejected for the transverse momenta above 25 MeV/c.

(ii) A K_S^0 fit was selected if the negative-track transverse momentum was greater than 105 MeV/c.

(iii) The $\bar{\Lambda}$ fit was only selected if its χ^2 probability was at least three times that of the competing fits. This criterion was chosen to keep the ratio of ambiguous $\bar{\Lambda}$ fits to ambiguous K_S^0 and Λ fits the same as the overall numbers of $\bar{\Lambda}$, K_S^0, and Λ fits in order to avoid too large a ratio of ambiguous to unambiguous $\bar{\Lambda}$ fits. One event was assigned to a $\bar{\Lambda}$ decay by this criterion.

(iv) K_S^0/Λ ambiguities were resolved by satisfying two conditions: The ratio of K_S^0 decays with transverse π^- momentum below 105 MeV/c to

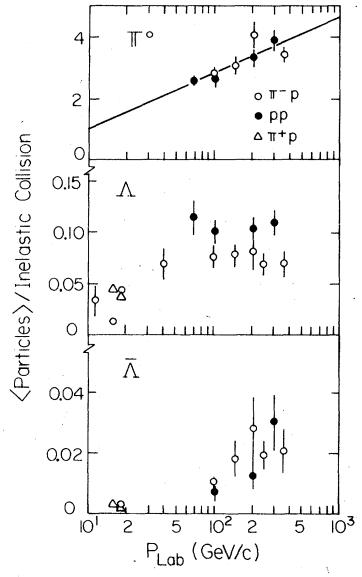

FIG. 5. Energy dependence of multiplicity of π^0, Λ, and $\bar{\Lambda}$ particles in $\pi^- p$, pp, and $\pi^+ p$ collisions. The straight line in the π^0 plot is from Whitmore (Ref. 5).

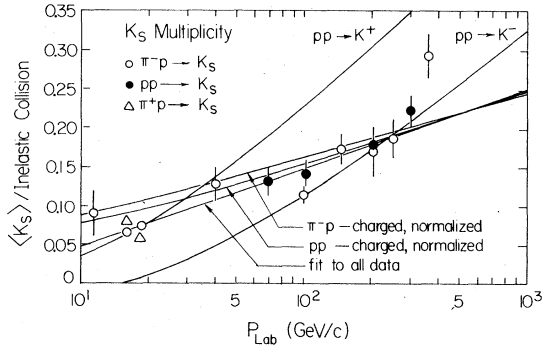

FIG. 6. Energy dependence of multiplicity of K_S particles in $\pi^- p$, pp, and $\pi^+ p$ collisions. A fit to all the data of the form $\langle n_k \rangle = A + B \ln s$ is shown. Fits of more complicated form to charged-particle multiplicities are shown for comparison, normalized as explained in the text. $K^\pm$ production fits are from Antinucci *et al.* (Ref. 8) and Stix and Ferbel (Ref. 7).

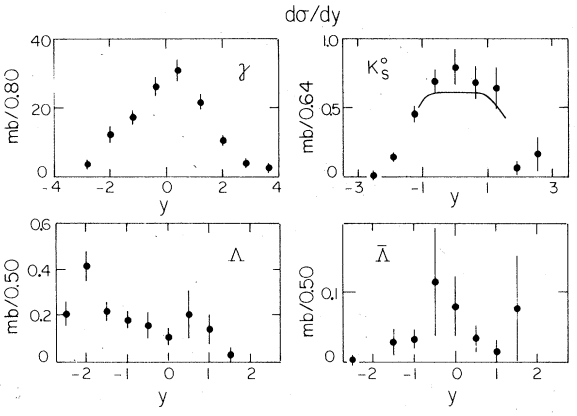

FIG. 7. Inclusive distributions (weighted) for K^0_S, Λ, $\bar{\Lambda}$, and γ production in $\pi^- p$ collisions at 147 GeV/c The distributions are shown as invariant cross section $d\sigma/dy$ vs c.m. rapidity y; errors are statistical only The "plateau" line in the K^0_S plot shows the height of the rapidity plateau predicted (see text) from the slope of the fit to the previous figure.

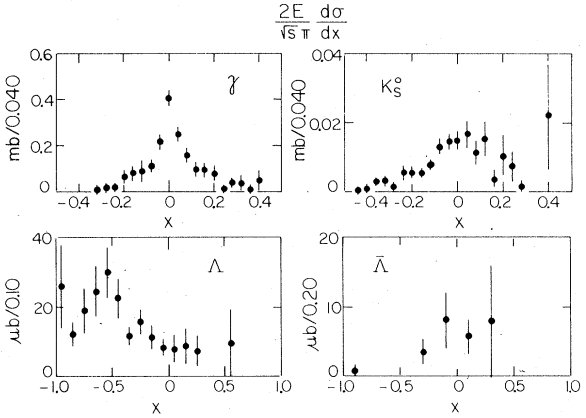

FIG. 9. Inclusive distributions for K^0_S, Λ, $\bar{\Lambda}$ production in $\pi^- p$ collisions at 147 GeV/c The distributions are shown as invariant cross section $(2E/\sqrt{s}\pi)\, d\sigma/dx$ vs Feynman x; errors are statistical.

those above 105 MeV/c should be given by the theoretical value of 14% for a spinless decay; secondly, we should expect K^0_S decays to simulate a $\bar{\Lambda}$ decay as often as a Λ decay. Both conditions could not be satisfied simultaneously, so we have resolved the K/Λ ambiguities so that neither condition is badly violated. The criterion for a K^0_S decay, then, is that the K^0_S fitted probability is greater than 1.43 times that of the Λ fit; this choice resolves 56 ambiguous neutrals into 46 Λ fits and 10 K^0_S fits.

Cross sections and distributions have been calculated in the usual fashion by assigning weights to neutrals to correct for their detection efficiency. The average detection weights were K^0_S: 2.03, Λ: 2.12, $\bar{\Lambda}$: 2.77, γ: 55.4. Other weighting factors accounted for the branching ratios of decays and for the method of partial remeasurement described earlier. Conversion to cross section, viz μb/event, were taken from Ref. 3 (1.43 μb/event for 2 prongs, 1.59 μb/event for other prongs).

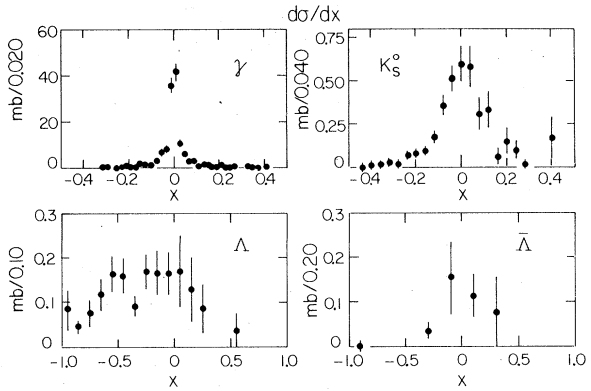

FIG. 8. Inclusive distributions for K^0_S, Λ, $\bar{\Lambda}$, and γ production in $\pi^- p$ collisions at 147 GeV/c. The distributions are shown as cross section $d\sigma/dx$ vs Feynman x; errors are statistical only.

As a check on quality of data, the decay-angle distributions for K^0_S, Λ, and $\bar{\Lambda}$ and the negative-track transverse-momentum distributions of all four neutral types are shown in Figs. 3 and 4. The decay angles, Fig. 3, are obtained in the particles' rest frame with z along the direction of the neutral, and x perpendicular to the camera axis, and are calculated for the negative-decay particle. They are acceptably flat in both angles for K^0_S and Λ and in azimuth angle for $\bar{\Lambda}$ as expected—there is little sign of the usual loss at azimuthal angle $=\pm\pi/2$. Figure 4 shows the momentum component of the negative track transverse to the line of flight of the neutral; again the experimental distributions agree with expected distributions.

III. CROSS SECTIONS AND INCLUSIVE DISTRIBUTIONS

Inclusive cross sections are shown in Table II. The Λ cross section includes Λ production from Σ^0 decays. Errors shown are mainly statistical but include contributions from estimates of contamination and of the reliability of weighting schemes. Contamination has been checked by looking for K^0_S, Λ, $\bar{\Lambda}$, and γ invariant-mass enhancements in each of the alternative categories. The worst cases were for $\bar{\Lambda}$ where 10% of the events could be γ contamination, and γ where $\frac{1}{2}$% of the K^0_S events could have been misclassified as γ's. These contaminations are small compared to the statistical error. The weighting

TABLE III. Central-region cross sections.

	$d\sigma/dy$ at $y=0$ (mb)	$(1/\sigma_{\text{Pomeron}})\ (1/\pi)d\sigma/dy$
K_S^0	1.24 ± 0.19	0.0178 ± 0.0027
Positive particles	17.5 ± 1	0.252 ± 0.015
Negative particles	16.0 ± 1	0.230 ± 0.015
Total charged	33.5 ± 1.4	0.482 ± 0.021
Λ	0.31 ± 0.11	0.0045 ± 0.0015
$\bar{\Lambda}$	0.20 ± 0.10	0.0029 ± 0.0015

schemes, including effects of decay volume, are estimated to contribute 5% uncertainties in the cross sections. Two-particle inclusive cross sections are also given in Table II.

Comparison of the cross sections with those for pp collisions and for πp collisions at other energies is shown in the form of average multiplicity in Fig. 5 for Λ, $\bar{\Lambda}$, and γ production, and in Fig. 6 for K_S production. The fit to π^0 multiplicity $\langle\pi^0\rangle$ is from Whitmore[5] and, in Fig. 6, the fits to K_S multiplicity will be discussed below. The sources of the data are tabulated in Ref. 6. The cross sections from this experiment agree within the errors with the general trends shown in Figs. 5 and 6.

The general trends of the cross sections are for rising average multiplicity as energy increases for all particles, except for Λ's above laboratory momentum of 50 GeV/c. In addition πp and pp collisions agree, except for Λ production which is presumably influenced by the difference in baryon number in the initial πp and pp states. If we average the multiplicity of Λ's above laboratory momenta of 40 GeV/c, then the ratio is $(pp \to \langle\Lambda\rangle)/(\pi p \to \langle\Lambda\rangle) = 1.44 \pm 0.03$. If all Λ production was in the fragmentation region of protons then, naively, this ratio should be 2.0. From the value of the ratio quoted above, we conclude that about half of Λ production occurs from proton fragmentation, the rest from pion fragmentation and/or central region production.

The production of K_S particles may be analyzed by comparison to pion production which constitutes most of the charged-particle production. Figure 6 shows the average K_S multiplicity $\langle n_k\rangle$ as a function of laboratory momentum for $\pi^- p$, pp, and some $\pi^+ p$ collisions. A fit to the data of the form $\langle n_k\rangle = A + B \ln s$ gives the result

$$\langle n_k\rangle = (-0.086 \pm 0.011) + (0.045 \pm 0.003) \ln s .$$

The fit is shown in Fig. 6 and can be seen to represent the general tendency of the data in spite of a low confidence level (χ^2 of 47.5 for 13 degrees of freedom). Comparison to charged-particle production can be made by obtaining similar fits to charged-particle multiplicity $\langle n_c\rangle$ and scaling this multiplicity down by a ratio of K_S to charged-particle production; in this case the ratio was taken to be ratio of average multiplicities for this experiment $\langle n_k\rangle/\langle n_c\rangle = 0.175/7.40$. Figure 6 shows scaled down fits to $\langle n_c\rangle$ in $\pi^- p$ and pp interactions.[7,8] Note that these fits to both $\pi^- p$ and pp charged multiplicities allow nonlinear terms. It can be seen that K_S production is similar in $\pi^- p$ and pp collisions and that it is similar to the scaled-down charged-particle production except possibly at the highest energy in $\pi^- p$ collisions. The fits are dominated by their ln$s$ terms and this appears to be the main energy dependence for both charged and K_S multiplicities. Also shown in the graph for com-

TABLE IV. Comparison of properties of central-region production and cross-section increase.

	Charged particles	K_S^0	K_S^0/charged ratio
Particle density per unit of rapidity $\frac{1}{\sigma_{\text{inelastic}}} \times \frac{d\sigma}{dy}\Big\|_{y=0}$	1.60 ± 0.07	0.059 ± 0.01	(3.7 ± 0.6)%
Multiplicity increase per unit of rapidity $\Delta n/\Delta \ln s$	1.45 ± 0.03	0.045 ± 0.003	(3.1 ± 0.2)%

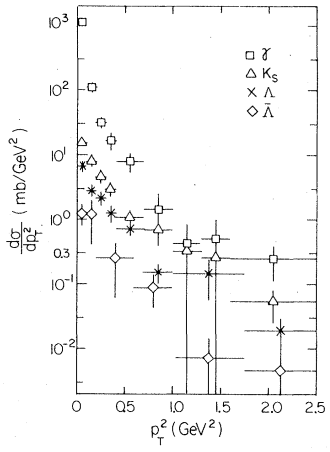

FIG. 10. Inclusive distributions for K_S, Λ, $\bar{\Lambda}$, and γ production in $\pi^- p$ collisions at 147 GeV/c The distributions are shown as cross section $d\sigma/dp_T^2$ vs transverse momentum squared p_T^2. The complete range of p_T^2 is shown.

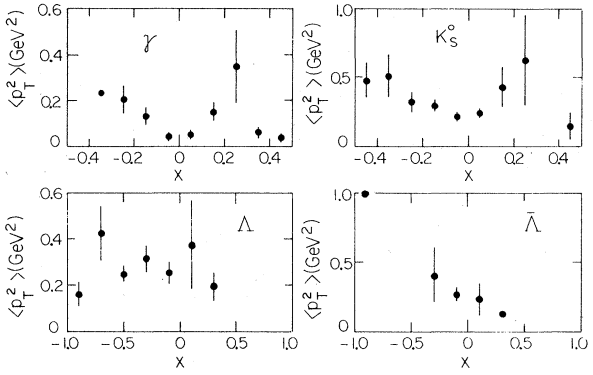

FIG. 12. Variation of average transverse momentum squared as a function of Feynman x for γ, K_S, Λ, and $\bar{\Lambda}$ particles in $\pi^- p$ collisions at 147 GeV/c. Note that in this and the following three figures, no error bar is shown for an average calculated from only one datum point.

parison purposes is a fit to $K^{\pm}$ multiplicities in pp collisions[8]; it can be seen that charged- and neutral-K multiplicities appear to have qualitatively different energy dependences.

The inclusive distributions of K_S^0, Λ, $\bar{\Lambda}$, and γ are shown as a function of c.m. rapidity y in Fig. 7, as a distribution in Feynman x in Fig. 8, and as the invariant cross section $2E/(\sqrt{s}\pi)d\sigma/dx$ in Fig. 9. From the distributions it can be seen that K_S^0, $\bar{\Lambda}$, and γ are produced predominantly in the central region of rapidity, whereas Λ's are produced predominantly in the fragmentation region of the proton target. The energy dependence and approach to scaling of the cross section $(1/\pi)(d\sigma/dy)$ at $y=0$ have been discussed by Boggild and Ferbel[9] and Whitmore[10] who assume a $s^{-1/4}$ asymptotic dependence for these cross sections normalized by a σ_{total} or σ_{pomeron}.[10] Our values for $d\sigma/dy$ and the normalized cross section are recorded in Table III for K_S^0 and for charged-particle production; they agree within errors with the expected behavior and other nearby data in Ferbel's and Whitmore's normalized plots.

For Fermilab energies it is difficult to establish the existence of a rapidity plateau even for pion production. For K_S production, we indirectly investigate the plateau by comparing the ln$s$ rise in K_S multiplicity with the ln$s$ expansion of the available rapidity and the height of the $d\sigma/dy$ distribution at $y=0$. Table IV shows the results tabulated as density of particle production per unit of rapidity vs multiplicity increase per unit of ln$s$. Figure 7 also shows the height of the central plateau expected from the multiplicity increase per unit of ln$s$. As can be seen from Table IV and Fig. 7,

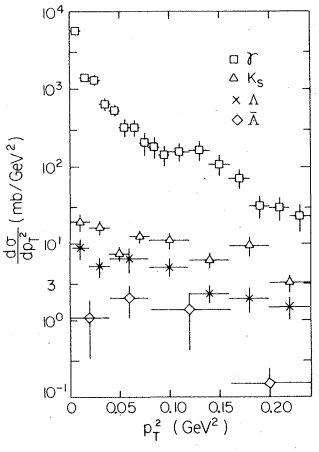

FIG. 11. Same transverse-momentum-squared distribution as previous figure but for narrow range of p_T^2.

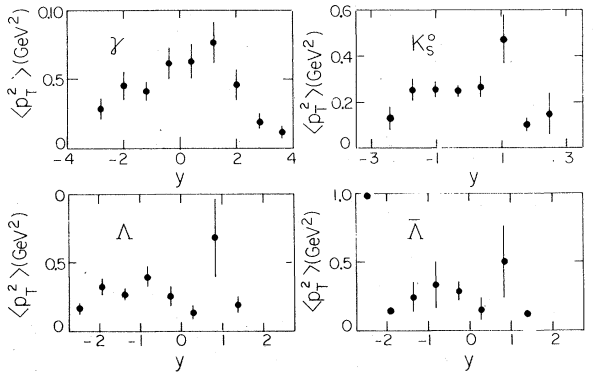

FIG. 13. Variation of average transverse momentum squared as a function of rapidity y for γ, K_S, Λ, and $\bar{\Lambda}$ particles in $\pi^- p$ collisions at 147 GeV/c

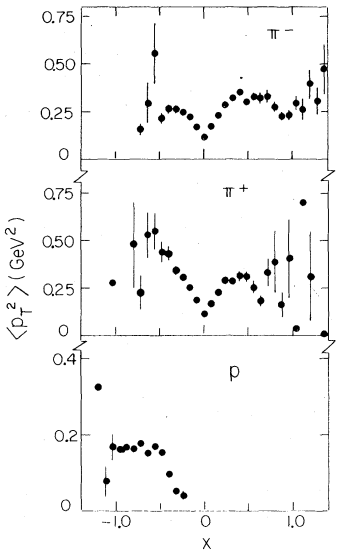

FIG. 14. Variation of average transverse momentum squared as a function of Feynman x for charged-particle production π^-, π^+, and p in $\pi^- p$ collisions at 147 GeV/c Note that protons are detected only up to 1.4 GeV/c in the laboratory frame.

there is rough parity between production in the central region and increases in multiplicity. Any differences are in the same direction as for charged-particle production. We conclude therefore that K_S production is consistent with the existence of a rapidity plateau.

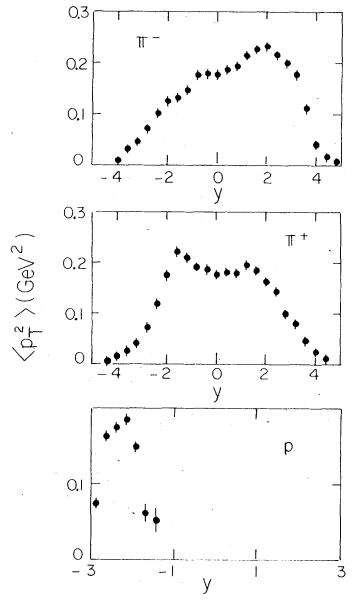

FIG. 15. Variation of $p_T{}^2$ as a function of rapidity y for charged-particle production π^-, π^+, and p in $\pi^- p$ collisions at 147 GeV/c. Note that protons are detected only up to 1.4 GeV/c in the laboratory frame.

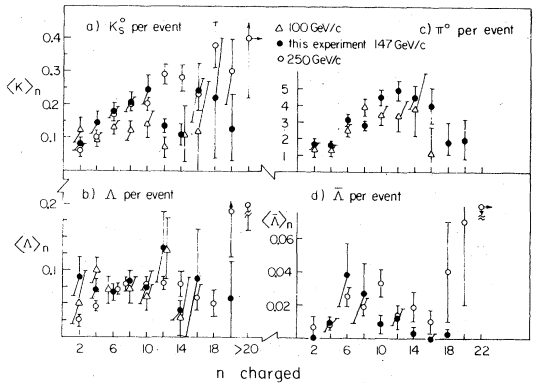

FIG. 16. Average multiplicity of K_S, Λ, π^0, and $\bar{\Lambda}$ particles as a function of associated charged multiplicity. Data from $\pi^- p$ collisions at 100 and 250 GeV/c are shown for comparison.

The transverse-momentum-squared distributions $d\sigma/dp_T{}^2$ for the neutrals, shown in Fig. 10, and with an expanded scale in Fig. 11, are sharply cut off just as the charged particles are. At small $p_T{}^2$, the γ distribution falls faster than the strange particles which are not noticeably different from each other. At large $p_T{}^2$, all the distributions level off and are decreasing at about the same rate from 0.5 to 2.5 GeV^2.

The profiles of $\langle p_T{}^2 \rangle$ vs the Feynman x and rapidity y variables are shown in Figs. 12 and 13. The usual dip near $x = 0$ ("seagull effect") which appears in charged-particle profiles can be seen in the γ and K_S data. The charged-particle profiles are shown for comparison in Figs. 14 and 15. Replotting the $\langle p_T{}^2 \rangle$ profiles as a function of rapidity is known to remove the "seagull effect" dip in the central region for charged-particle data and the same can be seen to be true for the strange-particle data in Fig. 13. Λ and $\bar{\Lambda}$ behavior is different from K_S and γ behavior, but statistics are too limited to conclude more.

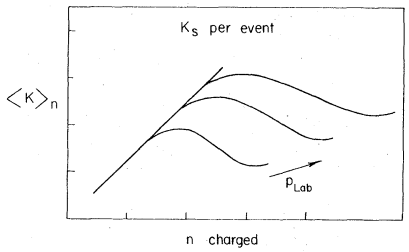

FIG. 17. Expected energy dependence of graph of average multiplicity of neutral particles vs associated charged multiplicity. The shape of the curve is assumed to be given and the energy dependence is derived in the text.

IV. MULTIPLICITIES OF NEUTRAL AND CHARGED PARTICLES

We discuss here only the correlation of neutral-particle multiplicity and associated charged-particle multiplicity. The dependence of charged-particle multiplicity on the mass of the recoil against the neutral particle is discussed elsewhere.[11]

It has been known for some time that the average number of neutral pions is correlated with the accompanying charged multiplicity from hadron collisions at Fermilab energies.[2] The same result is also known to apply to the production of K_S particles.[2] Figure 16 shows the average multiplicity[12] of π^0, K_S, Λ, and $\bar{\Lambda}$ as a function of accompanying charged multiplicity for this experiment. Also shown for comparison are 100- and 250-GeV/c data for $\pi^- p$ collisions. The usual strong correlation in K_S and π^0 data can be seen, but the correlation in the Λ data is uncertain as might be expected for baryon production.

The energy dependence of the associated neutral and charged multiplicities shown in Fig. 16 has been discussed in the form of a scaling function derived by Dao and Whitmore[13] from KNO arguments and applied to π^0 production by them, and to K_S production by Cohen,[14] both applications using only pp collision data. This scaling function uses the semi-inclusive cross section for the neutral-particle production and was quite well satisfied. We use an alternative scaling function based on the average multiplicity of neutral particles as a function of charged multiplicity (Fig. 16) since such a function is closely related to the more easily interpreted $K_S/\pi^{\pm}$ or $\pi^0/\pi^{\pm}$ ratio. We first present the new function then apply it to a compilation of both pp and πp data on the production of K_S, Λ, $\bar{\Lambda}$, and π^0 particles.

The KNO invariant distribution ψ for two types of particle (here taken to be charged and K_S to fix notation) is[15]

$$P_{nk} = \frac{1}{\langle n\rangle\langle k\rangle}\psi(z_n, z_k),$$

where $P_{nk} = \sigma_{nk}/\sigma_{\text{inelastic}}$, σ_{nk} = cross section for events with n charged particles and k neutral K_S particles, $z_n = n/\langle n\rangle$ and $z_k = k/\langle k\rangle$. The semi-inclusive K_S cross section is $\sum_k kP_{nk}\sigma_{\text{inelastic}}$ and the topological cross section is $\sum_k P_{nk}\sigma_{\text{inelastic}}$ so that the average multiplicity of K_S particles in n-prong events $\langle k\rangle_n$ is

$$\langle k\rangle_n = \langle k\rangle \frac{\sum_{z_k} z_k \psi(z_n, z_k)}{\sum_{z_k} \psi(z_n, z_k)}$$

$$= \langle k\rangle \phi_3(z_n),$$

where $\phi_3(z_n)$ is a scaling function, independent of s except as $\langle n\rangle$ depends on s in $z_n = n/\langle n\rangle$. The relation of this new invariant function ϕ_3 to that previously derived by Dao and Whitmore ϕ_2, and to the charged-particle invariant function of Koba, Nielsen, and Olesen[15] ϕ_1 is

$$\phi_3 = \phi_2/\phi_1.$$

A scaling plot can thus be made using $\langle k\rangle_n/\langle k\rangle$ vs $n/\langle n\rangle$.

Before inspecting data, a remark can be made about the energy dependence of the plot of n-prong average multiplicity of K_S particles $\langle k\rangle_n$ vs n. The energy dependence of the overall average K_S multiplicity $\langle k\rangle$ as we have seen above is approximately represented by

$$\langle k\rangle = a\langle n\rangle,$$

where a is a constant, and $\langle n\rangle$ increases approximately as ln$s$. Thus given a dependence of $\langle k\rangle_n$ on n at some energy, we expect the trend with increasing energy of the plot $\langle k\rangle_n$ vs n to be that shown in Fig. 17. Such a behavior has been noted before by Whitmore for π^0 production in pp collisions.[16]

Figures 18, 19, 20, and 21 show a compilation of πp and pp data[6] on K_S, π^0, Λ, and $\bar{\Lambda}$ production in the scaling plot of $\langle n_0\rangle_n/\langle n_0\rangle$ vs $n/\langle n\rangle$, where n_0 is the multiplicity of neutral particles. The data are restricted to be above laboratory momentum of about 70 GeV/c, but some lower-energy data are discussed below. Scaling is satisfied in the energy range allowed in the plot and $\pi^- p$ and pp data agree. It is worth noting that the range over

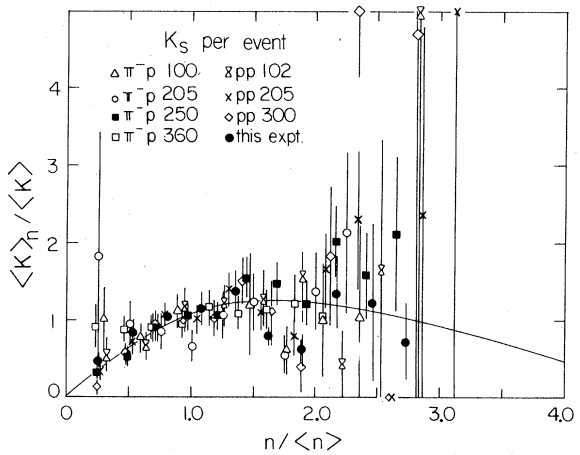

FIG. 18. Scaling form of plot of average multiplicity of K_S per event as a function of associated charged multiplicity. Abscissa and ordinate are normalized by $\langle n\rangle$ and $\langle k\rangle$ as derived in the text. A compilation of πp and pp data at various energies is shown, and a common hand-drawn curve is shown for reference in comparing K_S and π^0 data.

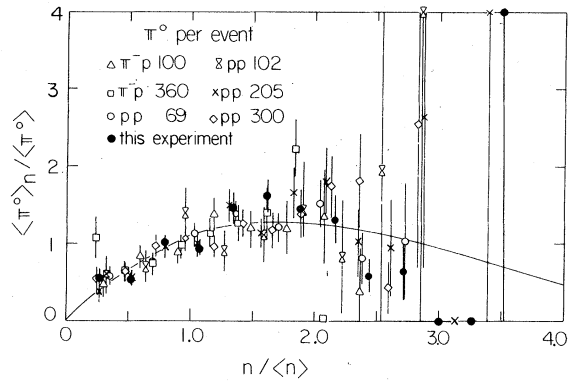

FIG. 19. Scaling form of plot of average multiplicity of π^0 per event as a function of associated charged multiplicity. Abscissa and ordinate are normalized by $\langle n\rangle$ and $\langle \pi^0\rangle$ as derived in the text. A compilation of πp and pp data at various energies is shown, and a common hand-drawn curve is shown for reference in comparing K_S and π^0 data.

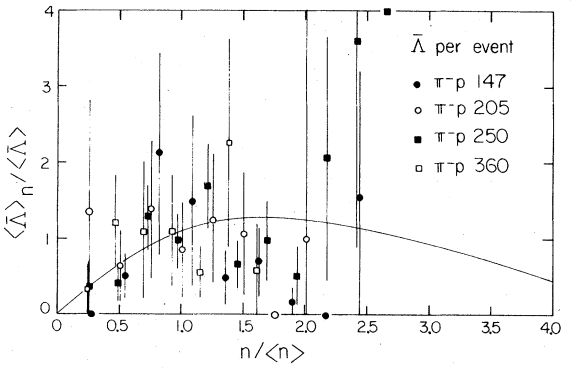

FIG. 21. Scaling form of plot of average multiplicity of $\bar{\Lambda}$ per event as a function of associated charged multiplicity Abscissa and ordinate are normalized by $\langle n\rangle$ and $\langle \bar{\Lambda}\rangle$ as derived in the text. Both πp and pp data are shown and the same hand-drawn curve is transferred from the K_S plot for comparison. Symbols for data points are the same as for Fig. 20.

which scaling can be checked is not extensive because of the ln$s$ dependence of the scaling factors $\langle n\rangle$ and $\langle n_0\rangle$; thus the range in $\langle n\rangle$ is 6.3 to 9.3, and the change in scaling factor is about 50%.

The scaling forms for K_S and π^0 data are similar and the same hand-drawn curve is added to both graphs to help in the comparison. Production of neutral and charged particles has been analyzed in several models, some of which[17] predict a reduction in neutral-particle production as the charged multiplicity increases above $n/\langle n\rangle = 1.0$. This clearly does not happen in the π^0 data. In the K_S data, however, there are some indications of a reduction[18] in K_S multiplicity around $n/\langle n\rangle = 1.5$ to 2.0, but not in the form suggested by the models and not in all experiments. The data are inclusive, but it is important to establish if there is a difference between K_S and π^0 production. A constant ratio K_S to charged-particle or π^0 to charged-particle multiplicity would appear as a straight line on the scaling curves. Neither K_S nor π^0 data show such a constant ratio.

Neutral-baryon production, i.e., Λ and $\bar{\Lambda}$ multiplicity, shown in Figs. 20 and 21, might be expected to differ from meson, K_S and π^0, production. Again, the same hand-drawn curve has been transferred from the K_S and π^0 multiplicity graphs to these Λ and $\bar{\Lambda}$ plots. Multiplicity of Λ's is less correlated with charged-particle multiplicity than for meson production. $\bar{\Lambda}$ production, however, appears to fall at multiplicities above the average.

For comparison to $K_S/\pi^\pm$ or $\pi^0/\pi^\pm$ ratios, we present in Figs. 22 and 23 the closely connected K_S and π^0

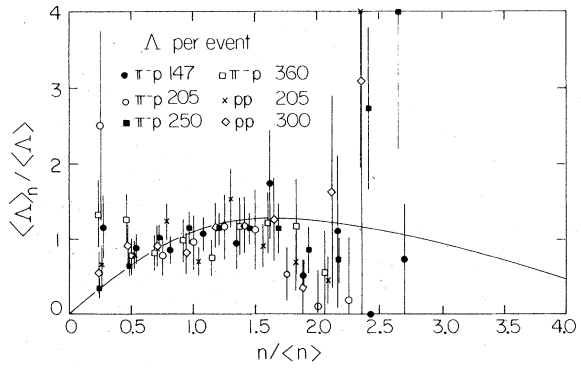

FIG. 20. Scaling form of plot of average multiplicity of Λ per event as a function of associated charged multiplicity. Abscissa and ordinate are normalized by $\langle n\rangle$ and $\langle \Lambda\rangle$ as derived in the text. A compilation of πp and pp data at various energies is shown and the same hand-drawn curve is transferred from the K_S plot for comparison.

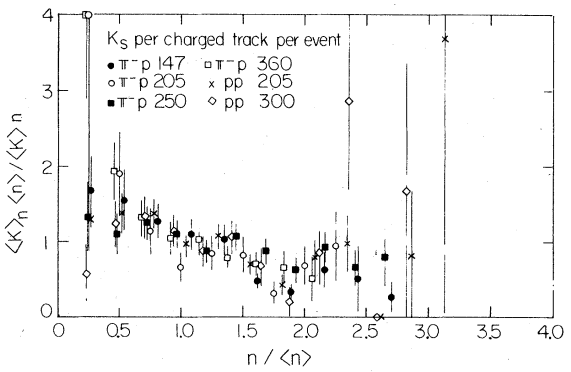

FIG. 22. Variation of a type of $K_S/\pi^\pm$ ratio with charged multiplicity-scaling form of K_S multiplicity per charged track vs scaling form of charged multiplicity. Symbols for data points are the same as for Fig. 20.

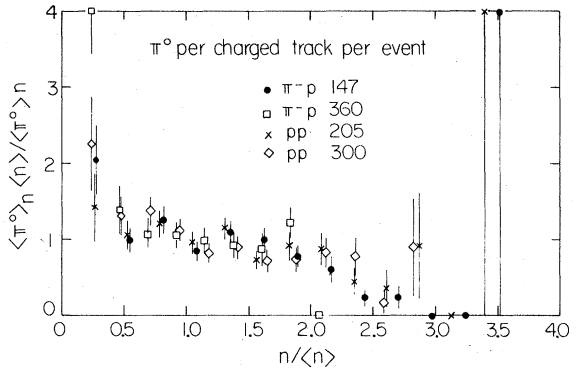

FIG. 23. Variation of a type of $\pi^0/\pi^{\pm}$ ratio with charged multiplicity-scaling form of π^0 multiplicity per charged track vs scaling form of charged multiplicity. Symbols for data points are the same as for Fig. 20.

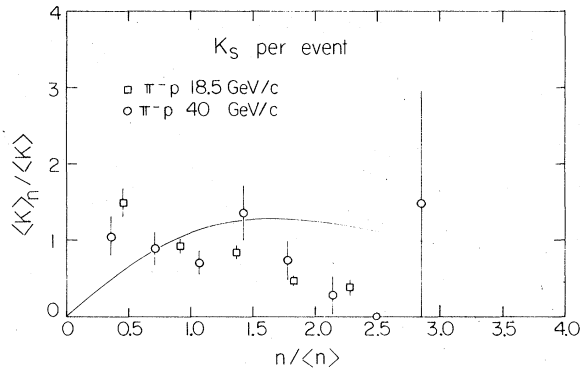

FIG. 24. Same scaling plot of average K_S multiplicity vs charged multiplicity as for Fig. 18 but including only lower-energy data for $\pi^- p$ collisions. The same hand-drawn curve as for previous figures is shown for comparison.

ratios to all charged particles still normalized by $\langle n_0 \rangle$ and $\langle n \rangle$ in order to keep the scaling properties previously derived. Both ratios fall with increasing charged multiplicity. The variables plotted are $(\langle n_0 \rangle_n / \langle n_0 \rangle)/(n/\langle n \rangle)$ vs $n/\langle n \rangle$.

Figure 24 presents some K_S data at low energies in the scaling plot for comparison to the high-energy data in Fig. 18. The same hand-drawn curve is again transferred to this lower-energy data in order to facilitate the comparison, and it can be seen that the low-energy data do not have the same shape as that of high energy.

ACKNOWLEDGMENTS

This work was supported in part by the U.S. Department of Energy and the National Science Foundation. We wish to thank the personnel of the Fermilab neutrino section and the 30-inch bubble-chamber facility whose skills and efforts made this experiment possible. We also thank the personnel of the participating universities and our data reduction personnel whose dedicated skills were vital to the success of this work.

*Present address: DESY, Hamburg, West Germany.
† Present address: New England Nuclear, Billerica, Massachusetts.
‡ Present address: Polytechnic Institute of New York, Brooklyn, New York.
§ Present address: Indiana University, Bloomington, Indiana.
‖ Present address: Purdue University, West Lafayette, Indiana.
¶ Present address: Argonne National Laboratory, Argonne, Illinois.
** Present address: Dialog Systems, Inc., Belmont, Massachusetts.
†† Present address: Duke University, Durham, North Carolina.
‡‡ Present address: Tel-Aviv University, Israel.
§§ Present address: Stanford Linear Accelerator Center, Stanford, California.
‖‖ Present address: Weizmann Institute of Science, Rehovot, Israel.
¶¶ On leave of absence from Tel-Aviv University, Israel.
*** Present address: Rockefeller University, N. Y. N. Y.
††† Present address: Fermilab, Batavia, Illinois.
‡‡‡ Present address: CERN, Geneva, Switzerland.

[1] Fermilab experiment E154.
[2] For compilations of data see J. Whitmore, Phys. Rep. 10C, 273 (1974); 27C, 187 (1976).
[3] D. Fong *et al*, Nucl. Phys. B102, 386 (1976).
[4] P. F. Jacques *et al*., Rev. Sci. Instrum. 48, 963 (1977).
[5] J. Whitmore, Phys. Rep. 27C, 187 (1976), Figs. 38, 39.
[6] Cross sections are from publications listed below. Inelastic cross sections are from the compilation by Particle Data Group, Rev. Mod. Phys. 47, 535 (1975). T. Ferbel and H. Taft, Nuovo Cimento 28, 1214 (1963); F. Barreiro *et al*., Phys. Rev. D 17, 669 (1978); P. Bosetti *et al*., Nucl. Phys. B94, 21 (1975); J. Bartke *et al*., Nuovo Cimento 24, 876 (1962); P. H. Stuntebeck *et al*., Phys. Rev. D 9, 608 (1974); J. T. Powers *et al*., *ibid*. 8, 1947 (1973); O. Balea *et al*., Nucl. Phys. B79, 57 (1974); H. Blumenfeld *et al*., Phys. Lett. 45B, 528 (1973); H. Blumenfeld *et al*., *ibid*. 45B, 525 (1973); V. V. Ammosov *et al*., *ibid*. 42B, 519 (1972); E. L. Berger *et al*., CERN Report No. CERN/D.Ph.II/Phys. 74-27, 1974 (unpublished); E. L. Berger *et al*., Nucl. Phys. B77, 365 (1974); J. W. Chapman *et al*., Phys. Lett. 47B, 465 (1973); C. Bromberg *et al*., Phys. Rev. Lett. 31, 1563 (1973); D. Ljung *et al*., Phys. Rev. D 15, 3163 (1977); K. Jaeger *et al*., *ibid*. 11, 2405 (1975); D. Bogert

et al., *ibid.* 16, 2098 (1977); S. Hagopian *et al.*, FSU Report No. HEP-76-1-2, 1976 (unpublished); A. Sheng *et al.*, Phys. Rev. D11, 1733 (1975); A. Firestone *et al.*, *ibid.* 10, 2080 (1974); V. P. Kenney *et al.*, in *Proceedings of the 19th International Conference on High Energy Physics, Tokyo, 1978*, edited by S. Homma, M. Kawaguchi, and H. Miyazawa (Physical Society of Japan, Tokyo, 1979); A. Firestone *et al.*, Phys. Rev. D 14, 2909 (1976).

[7]P. Stix and T. Ferbel, Phys. Rev. D 15, 358 (1977).

[8]M. Antinucci *et al.*, Lett. Nuovo Cimento 6, 121 (1973).

[9]H. Boggild and T. Ferbel, Annu. Rev. Nucl. Sci. 24, 451 (1974).

[10]Reference 5, Sec. 3.3. We have used σ (Pomeron) = (15.18 mb) $\times P_{\rm lab}^{0.0755}$ (where $P_{\rm lab}$ is in GeV/c) = 22.13 mb at 147 GeV/c.

[11]D. Brick *et al.*, Phys. Rev. D 19, 743 (1979).

[12]Average π^0 multiplicity is taken to be 0.5 $\times$ average γ multiplicity.

[13]F. T. Dao and J. Whitmore, Phys. Lett. 46B, 252 (1973).

[14]D. Cohen, Phys. Lett. 47B, 457 (1973).

[15]Z. Koba, H. B. Nielsen, and P. Olesen, Nucl. Phys. B40, 317 (1972).

[16]Figure 77 in J. Whitmore, Phys. Rep. 10C, 273 (1974).

[17]For example, G. H. Thomas, Phys. Rev. D 8, 3042 (1973); R. Kirschner, Nucl. Phys. B101, 507 (1975).

[18]Structure has been noted earlier by N. Yamdagni, CERN Report No. CERN/D.PhII/PHYS 75-40 (unpublished).

[19]Two-particle inclusive cross sections are for the process $\pi^- p \to a + b + X$, where X can contain a or b. When there are two or more identical particles of interest in the final state, the counting is done such that the inclusive cross section is the integral of the two-particle density function, e.g., a final-state 2γ contributes twice to $\sigma(\gamma\gamma)$, a state 3γ contributes six times to $\sigma(\gamma\gamma)$. Thus, $\sigma(aa) = \langle n_a (n_a - 1) \rangle \sigma_{\rm inel}$. The pair counts given in Table II, conversely, count pairs of particles without regard to permutation, e.g., final-state 3γ contributes a count of 3 to the $\gamma\gamma$ pair count.